Dynamic Pattern Formation in Electron-Beam-Induced Etching

Aiden A. Martin, Alan Bahm, James Bishop, Igor Aharonovich, and Milos Toth

Phys. Rev. Lett. **115**, 255501 — Published 15 December 2015

DOI: 10.1103/PhysRevLett.115.255501

Dynamic pattern formation in electron beam induced etching

Aiden A. Martin,[1,2] Alan Bahm,[1,3] James Bishop,[1] Igor Aharonovich,[1,*] and Milos Toth[1,†]

[1] *School of Mathematical and Physical Sciences, University of Technology Sydney, Ultimo, NSW, 2007, Australia*
[2] *Lawrence Livermore National Laboratory, Livermore, California 94550, USA*
[3] *FEI Company, 5350 Northeast Dawson Creek Drive, Hillsboro, Oregon 97124, USA*

(Dated: December 1, 2015)

We report highly ordered topographic patterns that form on the surface of diamond, span multiple length scales and have a symmetry controlled by the precursor gas species used in electron beam induced etching (EBIE). The pattern formation dynamics reveal an etch rate anisotropy and an electron energy transfer pathway that has been overlooked by existing EBIE models. We therefore modify established theory such that it explains our results and remains universally applicable to EBIE. The patterns can be exploited in controlled wetting, optical structuring and other emerging applications that require nano and micro-scale surface texturing of a wide bandgap material.

PACS numbers: 81.16.Rf, 81.16.Nd, 61.82.Fk, 68.43.Rs

Electron beam induced etching (EBIE) [1, 2] is a high resolution, single step, direct-write nanofabrication technique in which a precursor gas and an electron beam are used to realize etching. To date, EBIE has been used to study electron interactions with solids and adsorbates, and to machine a wide range of materials using etch precursors such as oxygen, water, ammonia, nitrogen trifluoride, xenon difluoride and chlorine. Key advantages of EBIE include cite-specificity, the absence of staining and severe damage inherent to focussed ion beam techniques, and the ability to etch materials such as diamond which are resistant to conventional chemical etch processes. Consequently, EBIE has recently been used to realize practical device components for use in photonics [3], plasmonics [4] and nanofluidics [5].

In this work, we report dynamic, highly ordered topographic patterns that form spontaneously on the surface of diamond during EBIE. Pattern formation is a ubiquitous process that provides fundamental insights into the roles of symmetry breaking, anisotropy and nonlinear interactions in emergent phenomena [6–8]. Here it reveals a chemical etch rate anisotropy that can not be explained by established EBIE theory. We therefore propose a fundamental modification, whereby the critical role of energetic electrons is to transfer energy to surface atoms of the solid rather than to surface-adsorbed precursor molecules. The new EBIE model is confirmed experimentally, explains the observed patterns, and resolves long standing problems that have been identified in the EBIE literature.

Fig. 1(a) is a schematic illustration of EBIE performed using H_2O precursor gas. Fig. 1(b) shows images of topographic patterns that form on the surface of single crystal (001) oriented diamond during H_2O EBIE performed at room temperature [9]. A movie showing the pattern formation and evolution dynamics is provided as Supplementary Video #1 [9]. The patterns were observed over a wide range of electron beam energy and flux of $2-10$ keV and $10^{17}-10^{22}$ cm^{-2}s^{-1}, respectively. Etching initiates at scratches and other surface defects, which expand laterally during EBIE, evolving into highly symmetric rhombohedra such as the large pit seen in the top left corner of Fig. 1(b). Similarly, the topography that is normally associated with surface roughness caused by EBIE rapidly evolves into step edges with {110} sidewalls which propagate laterally until they reach the edge of the area scanned by the electron beam. The {111} family of planes is absent from the resulting surface topography, the step sidewalls are comprised of {110} planes, and 90° step corners are formed at the intercepts of the {110} planes. Corner formation requires the (110), $(\bar{1}10)$, $(\bar{1}\bar{1}0)$ and $(1\bar{1}0)$ planes to etch slower than the (100), (010), $(0\bar{1}0)$ and $(\bar{1}00)$ planes. From these observations, we conclude that H_2O-mediated EBIE removes material from the {100} and {111} planes faster than from the {110} family of planes.

In order to prove conclusively that the proposed anisotropy yields the four-fold symmetry observed in Fig. 1(b), we used a 3D implementation of the level set method (LSM) [33]. LSM is a robust technique for evolving implicit surfaces under anisotropic velocity fields. It can be used to calculate surface shapes produced by anisotropies defined by differences between the etch rates of specific crystal planes. The simulations [9] reveal that the calculated surfaces match experiment only if the {110} planes that are oriented at 90° with respect to the electron beam axis etch slower than all other planes. Stable patterns are produced if the etch rate of the slowest etching planes to the remaining planes is at least 1:5. Supplementary Video #2 [9] and Fig. 1(d) show the resulting rhombohedral surface features.

Validity of the simulation was confirmed by applying the same etch rate anisotropy rule set to (111) oriented diamond. The simulation and H_2O EBIE both produced the trigons with {110} sidewalls shown in Fig. 1(c) and (e). The LSM simulations therefore support our conclusion that the geometries of patterns observed during H_2O EBIE of (001) and (111) oriented diamond is gov-

erned primarily by slow etching of specific {110} planes. However, this anisotropy can not be explained by conventional, established EBIE theory which is based on the assumption that the key role of energetic electrons is to dissociate physisorbed precursor molecules (e.g. H_2O) and thus generate reactive fragments (O^*) which react with surface atoms (C) to produce volatile molecules (CO) that desorb spontaneously, giving rise to localized chemical etching. In the specific case of H_2O EBIE of diamond, a possible pathway in this framework is the following [1, 2]:

$$H_2O_{[v]} \leftrightarrow H_2O_{[p]} \quad (1)$$

$$H_2O_{[p]} \xrightarrow{\Xi_1} H_2 + O^*_{[c]} \quad (2)$$

$$O^*_{[c]} + C_{[s]} \rightarrow C_{[s]}O_{[c]} \quad (3)$$

$$C_{[s]}O_{[c]} \xrightarrow{\Xi_2} CO_{[v]} \quad (4)$$

where the subscripts [v], [s], [p] and [c] signify vapor phase, solid phase, physisorbed and chemisorbed species, respectively. Reactions 1-4 represent adsorption of H_2O precursor molecules from the gas phase, dissociation of the adsorbates into fragments, bonding of oxygen fragments to the diamond surface, and desorption of CO, respectively (desorption of H_2 is not shown). Ξ_1 represents the energy barrier for dissociation of H_2O, and Ξ_2 is the binding energy of the reaction product. According to the standard EBIE model, Ξ_1 and Ξ_2 are overcome by a transfer of kinetic energy from the electrons that drive EBIE, and thermal energy of the substrate (kT), respectively. This model has been used to explain a wide range of experiments such as dependencies of etch rates on time, beam current density and pressure of the precursor gas [2, 5, 34–44]. However, the model can not explain the etch rate anisotropy seen in Fig. 1, unless different crystal planes give rise to significant variations in the electron dissociation cross-section of H_2O adsorbates, the secondary electron emission yield, or the local coverage of precursor molecule adsorbates. None of these are plausible since the precursor is H_2O, the patterns form at room temperature (and at elevated temperatures, as is discussed below), and the slowest etching planes are not consistently dark in secondary electron images.

To resolve the above issues, we propose a new mechanism, which proceeds through Reactions 1-4, but electrons provide the energy Ξ_2 in Reaction 4. Hence, the critical role of electrons is not to dissociate physisorbed precursor molecules, but to break bonds that bind surface atoms to the substrate and thus enable the desorption of the reaction products. During etching, Reaction 2 can reasonably be expected to proceed spontaneously since active (i.e. unterminated) surface sites are generated continuously during EBIE and interaction of H_2O molecules with a bare diamond surface results in spontaneous decomposition of H_2O [45] and formation of oxygen terminated sites. In this framework, the etch rate anisotropy needed to produce the patterns seen in Fig. 1 is not surprosing since Ξ_2 (i.e. the C-C bond properties and the corresponding cross-section for scission by electrons) is expected to vary with the crystal plane.

To confirm the proposed EBIE mechanism we performed an experiment based on the fact [46] that the C-C bonds are modified by hydrogen which reconstructs and stabilizes the {111} surface. We therefore performed H_2O EBIE of (001) and (111) oriented diamond in the presence of NH_3 gas, where the role of the NH_3 is to supply an excess of hydrogen radicals to terminate the (111) planes. Fig. 2 shows that the corresponding surface patterns consist of inverted pyramids and trigons, respectively, and that these geometries are indeed expected from LSM simulations in which the {111} planes are the slowest etching planes.

We performed one more experiment to further test the proposed EBIE mechanism. A consequence of the conventional EBIE model is that the etch rate should be directly proportional to the coverage of H_2O [1, 2] which is $\sim 4\times10^{-1}$ and 6×10^{-3} monolayers at 298 and 400 K, respectively, due to the temperature-dependence of the thermal desorption rate of H_2O. Hence, the etch rate of diamond is expected to be negligible at $\sim$ 400 K, as is shown in Fig. 3 (solid curves, calculated using the rate equation model presented in the Supporting Information [9]). However, the measured etch rate is approximately independent of temperature up to at least 600 K where it is over three orders of magnitude higher than that predicted by the conventional EBIE model, irrespective of the electron flux used in the simulations (the simulated flux was varied over five orders of magnitude because it affects adsorbate depletion and hence the predicted temperature-dependence of EBIE [1, 34]). The measurement is clearly inconsistent with the conventional model, but it is expected from the new model in which the etch rate is proportional to the concentration of chemisorbed oxygen. The lack of a temperature dependence therefore serves as direct evidence for the new EBIE model. Furthermore, the topographic patterns were observed at all temperatures that were investigated, as is illustrated by the image shown in the inset of Fig. 3. The abrupt step edges in the patterns generated at $\sim$ 600 K are inconsistent with any model that attempts to explain the etch rate anisotropy by spatial variations in the coverage of physisorbed adsorbates.

We note that the new EBIE model is consistent with all results in the literature that were explained successfully by the conventional EBIE model [1, 2, 5, 34–44, 47]. The scaling of etch rate with beam energy is the same because the secondary electron yield is proportional to the energy transferred from the beam to the surface atoms of the substrate. The beam current density and pressure play the same roles in the two models because both the physisorbed and chemisorbed adsorbates are consumed in EBIE, and replenished through the same mechanisms

(namely, adsorption from the gas phase and surface diffusion). Electron induced desorption of adsorbates plays the same role in each model [9, 34], and dependencies of etch rate on electron dose and time are are governed by the kinetics of the respective adsorbate concentrations. However, the new model provides a more compelling explanation for EBIE observed at cryogenic temperatures [35] since it does not require thermal desorption of the reaction products. Moreover, the new model is unique in being consistent with reports of UV laser induced etching of diamond, that is believed to proceed through a two photon C-C bond scission mechanism [8]. The new model also provides a satisfactory explanation for the fact that single crystal diamond can be etched by EBIE in the first place. The energy barrier of Reaction 4 in diamond is known to be significant [48] and therefore etching observed at room temperature, or any temperature below the onset of defect generation and graphitization cannot be accounted for in the standard model.

Finally, we note that anisotropic wet etching of diamond proceed through a graphitization pathway and the etch rate is limited by the anisotropic graphitization rate. However, the topographic patterns reported here cannot be explained by analogous damage generation mechanisms, or those encountered in conventional dry etch processes [49, 50] for a number of reasons. First, the EBIE rate anisotropy was modified significantly by the presence of NH_3 gas, which should not change the sub-surface damage generation rate. Second, pattern formation was either modified or suppressed entirely if residual hydrocarbon contaminants were present on the etched surface. Such contaminants are common in electron microscopes, alter the surface termination during EBIE, and give rise to a competing process of electron beam induced deposition of carbon [1]. The contaminants likely account for the fact that patterns have not been reported in prior EBIE literature (here, we suppressed contamination using the sample cleaning procedure detailed in the Supporting Information [9]). Third, prior studies of EBIE of single crystal diamond have failed to produce any evidence of damage by photoluminescence and Raman spectroscopy [3, 43, 51, 52]. Fourth, the generation rate of damage produced by a 5 keV electron beam scales with the local energy density deposited into the substrate throughout the electron interaction volume [47]. The damage generation rate is therefore isotropic, except for special cases where the electron beam axis is parallel to a channeling axis, which should produce a strong dependence of the patterns on sample tilt, which was not observed in our experiments. We therefore conclude that sub-surface damage generation does not play a role in the observed etching and pattern formation behavior.

To summarize, we showed several novel dynamic pattern formations on the surface of single crystal diamond. We proposed an amended model for the EBIE process that is based on interactions of electrons with the substrate rather than the precursor molecule adsorbates. Our results can be leveraged to engineer surface patterns controlled by electron beam irradiation conditions.

A portion of this work was funded by FEI Company and the Australian Research Council (Project Number DP140102721). A portion of this work was performed under the auspices of the U.S. Department of Energy by Lawrence Livermore National Laboratory under Contract DE-AC52-07NA27344. A.A.M. is the recipient of a John Stocker Postgraduate Scholarship from the Science and Industry Endowment Fund. I.A. is the recipient of an Australian Research Council Discovery Early Career Research Award (Project Number DE130100592). A.B. is grateful to Branislav Radjenovic and Ian Mitchell for insightful discussions of etch rate interpolation techniques and the level set method. A.A.M. and A.B. contributed equally to this work.

* Igor.Aharonovich@uts.edu.au
† Milos.Toth@uts.edu.au

[1] I. Utke, S. Moshkalev, and P. Russell, *Nanofabrication Using Focused Ion and Electron Beams: Principles and Applications* (Oxford University Press, New York, 2012).
[2] M. Toth, Appl. Phys. A Mater. Sci. Process. **117**, 1623 (2014).
[3] A. A. Martin, M. Toth, and I. Aharonovich, Sci. Rep. **4**, 5022 (2014).
[4] J. B. Lassiter, M. W. Knight, N. A. Mirin, and N. J. Halas, Nano Lett. **9**, 4326 (2009).
[5] J. M. Perry, Z. D. Harms, and S. C. Jacobson, Small **8**, 1521 (2012).
[6] M. C. Cross and Hohenberg, P.C., Rev. Mod. Phys. **65**, 851 (1993).
[7] S. Kondo and T. Miura, Science **329**, 1616 (2010).
[8] A. Lehmann, C. Bradac, and R. P. Mildren, Nat. Commun. **5**, 3341 (2014).
[9] See Supplemental Material [URL], which includes Refs. [10–32], for videos of pattern formation and detailed descriptions of the experimental and modeling methodologies.
[10] G. D. Danilatos, Adv. Electron. El. Phys. **71**, 109 (1988).
[11] C. J. Lobo, A. Martin, M. R. Phillips, and M. Toth, Nanotechnology **23**, 375302 (2012).
[12] A. A. Martin, G. McCredie, and M. Toth, Appl. Phys. Lett. **107**, 041603 (2015).
[13] J. A. Sethian and D. Adalsteinsson, IEEE Trans. Semicond. Manuf. **10**, 167 (1997).
[14] J. A. Sethian, *Level Set Methods and Fast Marching Methods: Evolving Interfaces in Computational Geometry, Fluid Mechanics, Computer Vision, and Materials Science* (Cambridge University Press, New York, 1999).
[15] S. Osher and N. Paragios, *Geometric Level Set Methods in Imaging, Vision, and Graphics* (Springer, New York, 2003).
[16] O. Ertl, Numerical Methods for Topography Simulation, Ph.D. thesis, Technical University Vienna (2010).
[17] J. Bezanson, S. Karpinski, V. B. Shah, and A. Edelman, arXiv:1209.5145 (2012).

[18] T. J. Hubbard, *MEMS Design: The Geometry Of Silicon Micromachining*, Ph.D. thesis, California Institute of Technology (1994).

[19] B. Radjenović, J. K. Lee, and M. Radmilović-Radjenović, Comput. Phys. Commun. **174**, 127 (2006).

[20] B. Radjenović and M. Radmilović-Radjenović, Acta Phys. Pol., A **119**, 447 (2011).

[21] B. Radjenović, M. Radmilović-Radjenović, and P. Belicev, Int. Res. J. Pure Appl. Chem. **4**, 562 (2014).

[22] B. Radjenović and M. Radmilović-Radjenović, Thin Solid Films **517**, 4233 (2009).

[23] K. Sangwal, *Etching of Crystals: Theory, Experiment, and Application*, edited by S. Amelinckx and J. Nihoul, Defects in Solids, Vol. 15 (Elsevier, Amsterdam, 1987).

[24] U. Ayachit, *The ParaView Guide: A Parallel Visualization Application* (Kitware, 2015).

[25] P. Martineau, M. Gaukroger, R. Khan, and D. Evans, Phys. Status Solidi C **6**, 1953 (2009).

[26] K. Fichthorn and R. Miron, Phys. Rev. Lett. **89**, 196103 (2002).

[27] P. L. Dickrell, N. Argibay, O. L. Eryilmaz, A. Erdemir, and W. G. Sawyer, J. Tribol. **131**, 032102 (2009).

[28] J. Hagymassy, Jr., S. Brunauer, and R. S. Mikhail, J. Colloid Interface Sci. **29**, 485 (1969).

[29] J. Bishop, C. J. Lobo, A. Martin, M. Ford, M. Phillips, and M. Toth, Phys. Rev. Lett. **109**, 146103 (2012).

[30] J. Cullen, A. Bahm, C. J. Lobo, M. J. Ford, and M. Toth, J. Phys. Chem. C **119**, 15948 (2015).

[31] S. J. Randolph, A. Botman, and M. Toth, Part. Part. Syst. Charact. **30**, 672 (2013).

[32] K. P. Loh, X. N. Xie, S. W. Yang, and J. C. Zheng, J. Phys. Chem. B **106**, 5230 (2002).

[33] S. Osher and R. Fedkiw, *Level Set Methods and Dynamic Implicit Surfaces* (Springer, New York, 2003).

[34] M. Toth, C. J. Lobo, V. Friedli, A. Szkudlarek, and I. Utke, Beilstein J. Nanotechnol. **6**, 1518 (2015).

[35] A. A. Martin and M. Toth, ACS Appl. Mater. Interfaces **6**, 18457 (2014).

[36] F. J. Schoenaker, R. Córdoba, R. Fernández-Pacheco, C. Magén, O. Stéphan, C. Zuriaga-Monroy, M. R. Ibarra, and J. M. De Teresa, Nanotechnology **22**, 265304 (2011).

[37] S. Randolph, M. Toth, J. Cullen, C. Chandler, and C. Lobo, Appl. Phys. Lett. **99**, 213103 (2011).

[38] N. Vanhove, P. Lievens, and W. Vandervorst, J. Vac. Sci. Technol. B **28**, 1206 (2010).

[39] H. Miyazoe, I. Utke, J. Michler, and K. Terashima, Appl. Phys. Lett. **92**, 043124 (2008).

[40] M. G. Lassiter and P. D. Rack, Nanotechnology **19**, 455306 (2008).

[41] Y. R. Choi, P. D. Rack, B. Frost, and D. C. Joy, Scanning **29**, 171 (2007).

[42] P. D. Rack, S. Randolph, Y. Deng, J. Fowlkes, Y. Choi, and D. C. Joy, Appl. Phys. Lett. **82**, 2326 (2003).

[43] J. Taniguchi, I. Miyamoto, N. Ohno, K. Kantani, M. Komuro, and H. Hiroshima, *Jpn J Appl Phys 1*, Jpn. J. Appl. Phys. **36**, 7691 (1997).

[44] H. Fujioka, K. Nakamae, M. Hirota, K. Ura, N. Tamura, and T. Takagi, J. Phys. D **23**, 266 (1990).

[45] A. Laikhtman, A. Lafosse, Y. L. Coat, R. Azria, and A. Hoffman, Surface Science **551**, 99 (2004).

[46] R. Klauser, J.-M. Chen, T. J. Chuang, L. M. Chen, M. C. Shih, and J. C. Lin, Surf. Sci. **356**, L410 (1996).

[47] A. A. Martin, M. R. Phillips, and M. Toth, ACS Appl. Mater. Interfaces **5**, 8002 (2013).

[48] M. Frenklach, D. Huang, R. E. Thomas, R. A. Rudder, and R. J. Markunas, Appl. Phys. Lett. **63**, 3090 (1993).

[49] Z. Shpilman, I. Gouzman, E. Grossman, L. Shen, T. K. Minton, J. T. Paci, G. C. Schatz, R. Akhvlediani, and A. Hoffman, J. Phys. Chem. C **114**, 18996 (2010).

[50] P. Olivero, S. Rubanov, P. Reichart, B. C. Gibson, S. T. Huntington, J. Rabeau, A. D. Greentree, J. Salzman, D. Moore, D. N. Jamieson, and S. Prawer, Adv. Mater. **17**, 2427 (2005).

[51] J. Schwartz, S. Aloni, D. F. Ogletree, and T. Schenkel, New J. Phys. **14**, 043024 (2012).

[52] A. A. Martin, S. Randolph, A. Botman, M. Toth, and I. Aharonovich, Sci. Rep. **5**, 8958 (2015).

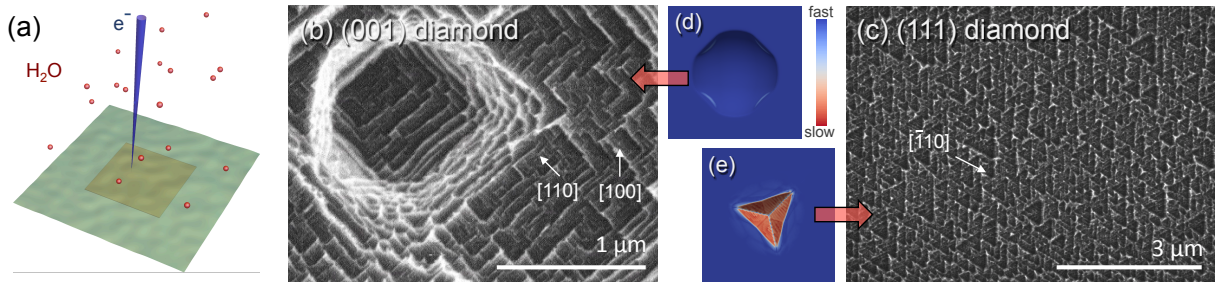

FIG. 1. Topographic patterns formed during H_2O mediated electron beam induced etching of single crystal diamond performed using a beam energy of 5 keV and a current of 34 nA. (a) Schematic illustration of H_2O EBIE. (b) Expanding rhombohedra formed on the surface of (001) oriented diamond, and (c) trigons on the surface of (111) diamond. (d,e) Corresponding simulated rhombohedra and trigons (colored by the relative local etch rate) that are expected if the {110} planes are the slowest etching planes.

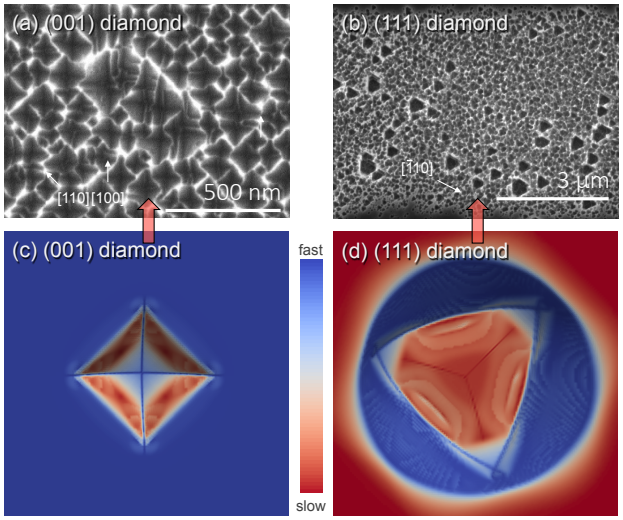

FIG. 2. Topographic patterns formed during electron beam induced etching of single crystal diamond in the presence of NH_3 (the electron beam parameters were the same as in Fig. 1). (a) Expanding inverting pyramids formed on the surface of (001) oriented diamond, and (b) trigons on the surface of (111) diamond. (c,d) Corresponding simulated pyramids and trigons (colored by the relative local etch rate) that are expected if the {111} planes are the slowest etching planes.

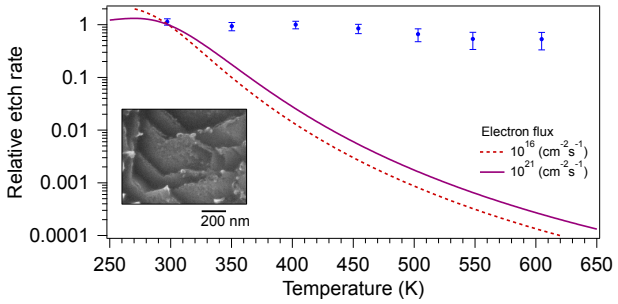

FIG. 3. Temperature dependence of the rate of EBIE measured experimentally (points) and calculated using the established EBIE model [9] (lines) using a wide range of electron fluxes. The etch rates are normalized to the EBIE rate at room temperature where the measured etch rate is $\sim 10^{-3}$ μm^{3}s^{-1}. The inset shows an image of surface topography generated by H_2O EBIE at ~ 600 K. EBIE experiments were performed using a beam energy of 5 keV, and an electron flux of $\sim 8 \times 10^{17}$ cm^{-2}s^{-1}.